

Aerosol Jet[®] Printing of Poly(3,4-Ethylenedioxythiophene): Poly(Styrenesulfonate) onto Micropatterned Substrates for Neural Cells In Vitro Stimulation

Miriam Seiti^{1,2}, Paola Serena Ginestra², Rosalba Monica Ferraro³, Silvia Giliani³,
Rosaria Maria Vetrano¹, Elisabetta Ceretti², Eleonora Ferraris^{1*}

¹Department of Mechanical Engineering, KU Leuven, 3001, Leuven, Belgium

²Department of Mechanical and Industrial Engineering, University of Brescia, 25123, Brescia, Italy

³Department of Molecular and Translational Medicine, “Angelo Nocivelli” Institute for Molecular Medicine, University of Brescia, ASST Spedali Civili, Brescia, Italy

Abstract: In neural tissue engineering (NTE), topographical, electrical, mechanical and/or biochemical stimulations are established methods to regulate neural cell activities in *in vitro* cultures. Aerosol Jet[®] Printing is here proposed as enabling technology to develop NTE integrated devices for electrically combined stimulations. The printability of a poly(3,4-ethylene dioxythiophene):poly(styrenesulfonate) (PEDOT: PSS) commercial ink onto a reference substrate was firstly investigated and the effect of the process parameters on the quality of printed lines was analyzed. The study was then extended for printing thick electrodes and interconnects; the print strategy was finally transferred to a silicon-based wafer with patterned microchannels of proven cellular adhesion and topographical guidance. The results showed values of electrical resistance equal to $\sim 16 \Omega$ for printed electrodes which are $\sim 33 \mu\text{m}$ thick and $\sim 2 \text{mm}$ wide. The electrical impedance of the final circuit in saline solution was detected in the range of 1 – 2 k Ω at 1 kHz, which is in line with the expectations for bioelectronic neural interfaces. However, cells viability assays on the commercial PEDOT: PSS ink demonstrated a dose dependent cytotoxic behavior. The potential cause is associated with the presence of a cytotoxic co-solvent in the ink’s formulation, which is released in the medium culture, even after a post-sintering process on the printed electrodes. This work is a first step to develop innovative *in vitro* NTE devices via a printed electronic approach. It also sheds new insights the transfer of AJ[®] print strategies across different substrates, and biocompatibility of commercial PEDOT: PSS inks.

Keywords: Printing of electronics; Aerosol Jet[®] printing; Conductive polymers; Biomedical; Neural tissue engineering

*Correspondence to: Eleonora Ferraris, Manufacturing Processes and Systems, Department of Mechanical Engineering, KU Leuven, Sint Katelijne Waver, 2860, Belgium; eleonora.ferraris@kuleuven.be

Received: November 3, 2021; **Accepted:** December 20, 2021; **Published Online:** January 28, 2022

(This article belongs to the *Special Section: 3D Printing and Bioprinting for the Future of Healthcare*)

Citation: Seiti M, Ginestra PS, Ferraro RM, *et al.*, 2022, Aerosol Jet[®] Printing of Poly(3,4-Ethylenedioxythiophene): Poly(Styrenesulfonate) onto Micropatterned Substrates for Neural Cells In Vitro Stimulation. *Int J Bioprint*, 8(1):504. <http://doi.org/10.18063/ijb.v8i1.504>

1. Introduction

Neurodegenerative diseases affect millions of people worldwide. According to the Alzheimer’s Disease International Report of 2019, people affected by dementia only is expected to reach 152 million by 2050. This is related with the increased aging of the global population. One of the causes of brain neurodegenerative diseases is the progressive dysfunction and limited self-repair of the

central nervous system. Although some symptoms can be relieved, there are still limited treatments to cure or slow down the progression of neurological disorders.

In this context, neural tissue engineering (NTE) can offer innovative solutions. NTE is a sub-domain of tissue engineering (TE), and it is defined as a multidisciplinary field enabling to develop biomimetic environment of the nervous system to study neural activities, aiming at

repairing and/or regenerating neural cells and tissues. In particular, NTE *in vitro* concepts have been established as an efficient and ethical alternative to *in vivo* studies. *In vitro* smart bio-architectures, namely (neural) scaffolds, can be indeed developed to recreate, for instance, a biomimetic brain extra cellular matrix in laboratory to investigate mechanisms, such as cellular differentiation, degeneration or regeneration, offering new possibilities for disease modelling and/or personalized medicine^[1]. Neural differentiation, as from induced pluripotent stem cells (iPSCs), can be modulated or accelerated using various (combined) stimuli, such as topographical, electrical, mechanical, or biochemical stimuli, which are known as axon guidance cues^[2]. As an example, micro-/nano-structured scaffolds, such as channelled substrates, have demonstrated to enhance directional guidance for neural networks growth. Electrical stimulation (ES) of iPSCs in culture medium is also known to influence direction and triggering of neurite outgrowths^[3]. Microelectrode arrays (MEAs) are currently the most widely adopted devices for combined digital neural electrophysiological activity stimulation and also recording. However, current MEAs solutions are not integrated into TE oriented substrates, and the majority of them are fabricated with flat electrodes on stiff substrates, which do not reassemble the complex three-dimensional (3D) neural architecture. Hence, these devices usually lack a 3D structure and do not allow the mimicking of axonal guidance.

In this context, Aerosol Jet® Printing (AJ®P) can provide new opportunities. AJ®P, which is an additive manufacturing technology commercialized by Optomec®, is able to fabricate printed electronics (PE) applications on various substrates (interconnects, electrodes, antennas, resistive and capacitive sensors, RFID, electrochemical sensors, etc.)^[4-7]. It is a nozzle-based direct writing technology, and it makes use of a functional ink, which is atomized into an aerosol mist (gas suspension of micro-sized material droplets) through piezoelectric ultrasonic or pneumatic methods. The mist is then transferred to the deposition head through a (nitrogen, N₂) carrier gas and focused in the nozzle into a high dense aerosol beam by means of an annular (N₂) sheath gas. As such, microscale resolutions down to 10 µm in width and ~100 nm in thickness can be attained via AJ®P. Moreover, functional nanoinks with a wide range of viscosity (1 – 100 mPas) can be printed, including conductive, dielectrics and biological solutions, such as metal loaded inks (particle size ≤ 0.5 µm)^[8,9], polymer^[10] or carbon-based solutions^[11,12], and hydrogels (as for collagen^[13,14]). Furthermore, it can print theoretically on any substrate displaying a certain surface energy, such as smooth/rough supports, flexible foils, textile, or papers, including free form parts, because of the variable stand-off distance (i.e., the distance 1 – 5 mm, between the tip of the nozzle

and substrate). AJ®P 3D micro-structuring has also been proven recently^[15-17], in which different inks composed of silver nanoparticles (AgNPs), polymers (PEDOT: PSS) or biological (collagen) dispersions, were exploited for the fabrication of 3D micropillars and lattice structures.

In this study, poly(3,4-ethylenedioxythiophene): poly(styrenesulfonate) (PEDOT: PSS) electrodes and interconnects, up to 30 mm thick, are AJ® printed on a microstructured silicon (Si)-based wafer with proven cellular adhesion, to develop a customized bioelectrical NTE *in vitro* device with combined topographical and electrical axon guidance cues. To the author's knowledge, this combination of material, substrate and application is unique in the literature. PEDOT: PSS was selected for this study because of its known good conductivity, biocompatibility, and electrochemical stability, when it is mixed with specific co-solvents and additives^[18]. Several examples of PEDOT: PSS inks have also been already reported in the literature for bioelectrical neural applications^[3,19-21]. Despite the guidelines and experimental framework about the optimization of AJ®P printing parameters^[22-24], the literature focuses on the typically empirical approaches specifically oriented to a given combination of ink solution and substrate, such as silver ink combined with flat/flexible supports. Moreover, they lack in generality and applicability, for example, when dealing with micro-structured substrates. Furthermore, they usually refer to thin printed patterns for the purpose of PEs, instead of thick designs for multifunctional applications, such as bioelectronics interfaces. In this paper, the use of a generalized print transfer methodology is proposed instead. It is based on the concept of wettability as indication of the substrate-ink interaction. Hence, the printability of the selected ink was firstly investigated on a substrate of reference (glass slides) and optimized for the desired purpose (thick printed interconnects and electrodes). The print strategy was then transferred to the substrate of interest, previously treated to match the wettability of the reference support, hence reducing the time and cost of investigation and process optimization. In addition, a manual and automated detection protocol, based on quantitative and qualitative data, was proposed. The printed lines characterized with respect to accuracy and geometrical profiles, electrical conductivity and biocompatibility, and interesting new insights concerning the cytotoxicity of the selected PEDOT: PSS ink were reported. The electrical impedance of the final device was eventually tested in saline solution.

2. Materials and methods

2.1. Inks and substrates

A PEDOT: PSS inkjet ink (ORGACON™ Transparent Conductive Inkjet Ink IJ-1005 AGFA NV, BE) was used

as AJ[®]P material. It is a water-based solution with 0.8 wt% solid content, and 12 – 20 wt% diethylene glycol (DEG) as co-solvent. The ink viscosity, η_{INK} , is within 7 – 12 mPas, the surface tension, s_{INK} , within 31 – 34 mN/m, and the surface resistance, r_{INK} , around 800 Ω/sq . These properties are within the limits of AJ[®]P inks. The use of most commonly applied AJ[®]P inks, such as AgNPs suspensions, was excluded in this work. With exception of their renowned antibacterial properties, AgNPs inks can have undesirable side effects in *in vitro* bioelectrical applications, such as oxidative stress and cellular damage, caused by the release of Ag^+ ions in the medium culture^[25]. For example, the AJ[®] SI-AJ20x (AGFA NV, BE) composed of AgNPs at 10 – 20 wt%, was identified as high cytotoxic in the presence of neuronal cells^[26].

Glass slides (Superfrost VWR, BE) were selected as reference substrates for AJ[®]P investigations, while the NTE substrates were pyrolyzed Si wafers with patterned microchannels of proven topographical guidance on the alignment of neurites outgrowth^[27]. Specifically, the substrate was fabricated according to the protocol reported by Ferraro *et al.*^[27], in which micropatterned channels were produced by spin coating and ultraviolet exposure of a SU-8 photoresistor via photolithography process. Subsequently, the substrate was subjected to a pyrolysis treatment (Step 1: 270°C for 3 h, Step 2: Ramp of 10°C/min till 950°C in inert atmosphere) to obtain the final glassy carbon microchannels. Moreover, the NTE scaffolds were electrically insulated by plasma coating with a Parylene-C layer (film thickness $\sim 4 \mu\text{m}$). The biocompatibility of Parylene-C is well recognized in the literature, mostly for the encapsulation of bioelectronic

interfaces^[28,29]. The average thickness, t , and width, w , of the microchannels after coating were measured by a laser probe profilometer (PF60[®] Profilometer, Mitaka), and they resulted in a $t_{\text{avg}} = 33.3 \pm 0.1 \mu\text{m}$ and a $w_{\text{avg}} = 27.4 \pm 4.2 \mu\text{m}$, respectively. **Figure 1** reports representative extracts of the profilometer graphs obtained, along with t and w values, before and after coating. An optical image of the final Parylene-C-coated Si channel is also presented. Before use, all substrates were cleaned with distilled water (DI) and 2-propanol (IPA, Sigma Aldrich, BE), in an ultrasonic bath at $T = 25^\circ\text{C}$ (EMMI - 20 HC, Emag) for 10 min.

2.2. Process investigation

Printing was conducted on an AJ[®]P 300s system equipped with the ultrasonic configuration (Optomec[®], USA). **Table 1** lists the experimental campaigns performed in ambient conditions (22°C, 55%rh). The PEDOT: PSS inkjet ink was successfully sonicated for 10 min at 25°C, at a power atomization of 49.5 V. Ink refilling in the vial (850 μL) was performed around every 3 h to ensure continuous stable printing, and a clearance of ~ 5 min was taken thereafter to calibrate the printer and reduce system drifting. Glass slides were used as positive reference for process investigation and optimization. Before printing, the substrates were left on the platform for about 10 min to ensure thermal equilibrium with the temperature plate. A post-printing thermal curing was applied in oven for 8 min at $T = 150^\circ\text{C}$ (Heraeus oven) to ensure full evaporation of the solvent and ink sintering. The focusing ratio R_f (#), here defined as the

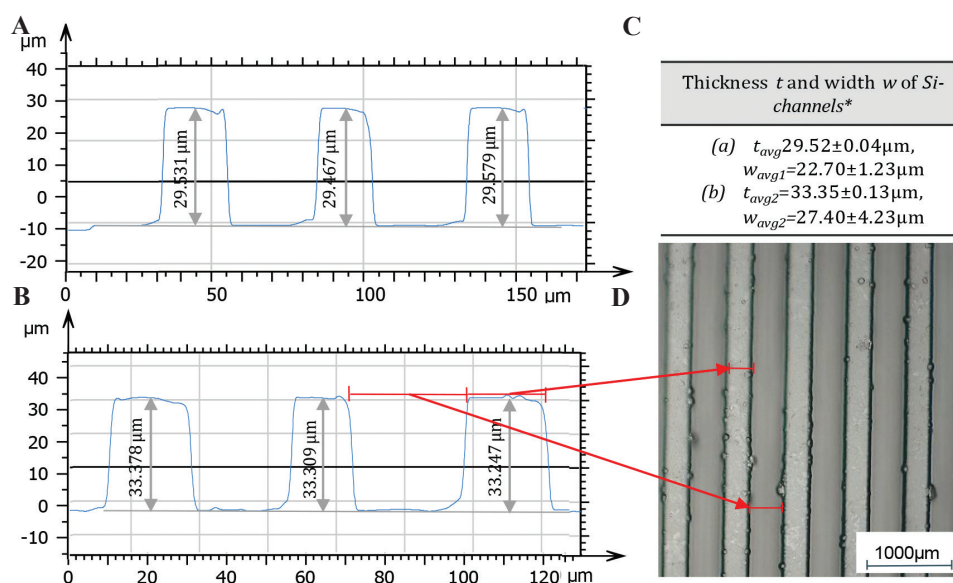


Figure 1. Optical profilometer analysis on Si-channels substrates before and after Parylene-C coating. The figure shows a profilometer extract (A) before and (B) after coating. (C) Values of mean thickness t and width w of Si-channels in both cases. (D) Representative optical image of the homogenous Parylene-C coating.

Table 1. Details of the experimental campaigns performed on the AJ[®]P of a PEDOT: PSS ink. The first campaign is related to the study of line quality by varying the focusing ratio and the platen temperature. The second one deals with the study of electrical resistance and thickness of printed samples, by varying the number of deposited layers (Platen temperature, $T=40^{\circ}\text{C}$)

1st experimental campaign on the quality of printed lines as a function of key process parameters																
Parameters		Values														
Substrate		Glass slides, VWR Superfrost [®] Plus Micro Slide														
Nozzle diameter \varnothing (μm)		300														
Stand-off distance z (mm)		3														
Printing speed s (mm/s)		25														
Number of layers n (#)		10														
Sample		1 printed line of length, $l=10$ mm														
Focusing ratio R_f (#)		1					1.5					2				
S (sccm)		10	20	30	40	50	15	30	45	60	75	20	40	60	80	100
A (sccm)		10	20	30	40	50	10	20	30	40	50	10	20	30	40	50
Platen temp. T ($^{\circ}\text{C}$)		25					40					60				
Response		Line quality q														
2nd experimental campaign on printing electrodes and interconnects as a function of the layer #																
Parameters		Values														
Sample		Interconnect					Electrode									
Layer n (#)		5	10	50	100	150	1	5	10	15	20	30	40	50		
R_f (S/A [sccm])		1 (40 – 40)			2 (80 – 40)		1 (40 – 40)			2 (80 – 40)			2 (80 – 40)			
Substrate		Glass					Glass					NTE substrate				
Response		Electrical resistance R										Thickness t				

ratio between the sheath gas flow, $S = (0 - 200)$ sccm, and carrier gas flow, $A = (0 - 50)$ sccm, along with the single contribution of these parameters, is a critical factor in AJ[®]P to ensure quality printing and high resolution. For a given nozzle diameter, it determines the size and shape quality of the aerosol beam, along with its particle distribution across the beam diameter. In particular, a convergent R_f ($R_f \geq 1$) is necessary to obtain a focused aerosol mist, with minimum presence of out of trajectory droplets depositing on the edges of the printed lines, and being responsible for the overspray phenomena. The platen temperature, T ($^{\circ}\text{C}$), and the number of deposited layers, n (#), are also important to build up thickness, achieve high conductivity and ensure print efficiency; the platen temperature, in particular, initiates the evaporation of the ink (co-) solvents (drying effect), and influences the ink behavior on deposition. Accordingly, a first experimental work was conducted to study the effect of the printing parameter focusing ratio, R_f , and the platen temperature, T , on the quality of single printed lines, q , as primary building element for electrical applications. The concept of the q parameter and its determination is explained in details in Section 2.2 (1). The focusing ratio was varied over three levels, $R_f = (1, 1.5, 2)$; each of them exploded into five sub-combinations of S and A , and then combined with three levels of platen temperature $T = (25,$

$40, 60)^{\circ}\text{C}$. Each experiment was repeated 3 times. Based on the knowledge acquired, suitable combinations of printing parameters for quality printing were identified, and a second experimental work was designed to study the effect of the number of deposited layers, n , and platen temperature, T , on the average electrical resistance, R_{avg} (Ω), and average thickness, t_{avg} (μm), of interconnects and electrodes. An interconnect is defined as a (single) track connecting two contact pads, while an electrode is a rectangular pad (e.g., 22×1 mm²), realized by printing consecutive layers of adjacent lines which overlap each other of a given quantity. When $T = 25^{\circ}\text{C}$, we instantly observed that the aerosol beam was too wet to support thick printing; on the contrary, when $T = 60^{\circ}\text{C}$, we noticed a significant shrinkage of the printed lines due to fast drying of the ink solvent, which compromised the printing stability, especially with increased n . For these reasons, the printing investigation was eventually implemented at 40°C only. The print strategy was eventually transferred to the NTE substrate of interest according to the methodology described in section 2.3. At least three printing repetitions were taken for each combination. Electrical resistances, R , of the printed elements were recorded by a two-point probe method (Digital Multimeter 73 III, Fluke). Four repetitions were taken for each sample. Eventually, an optical microscope

(Hirox KH – 8700) was used to inspect the quality and geometry of the printed features.

(1) Print quality

The line quality is a useful factor to determine whether the printed pattern is acceptable both in terms of shape accuracy and fidelity. It also helps to systematically explore the suitable process window for the desired purpose. The evaluation of the line quality is far from being trivial and several ways have been proposed in the literature^[22-24]. In this paper, a combined manual (visual inspection and operator’s rank (q)) and automated (image processing through MatLab program (q_a)) approach is presented to evaluate the line quality. In both cases, images of the printed lines were acquired through optical microscopy (Hirox KH – 8700). In this context, a good quality printed line is intended as a dense and well-defined track with straight edges and (almost) null overspray (i.e., scattered material, in the form of printed drops, deposited in the proximity of the line edges). Porous and sputtered lines are indeed difficult to control over shape and are not electrically functional. A reduction in the overspray also prevents wastage of ink, which is in most of the cases very precious and expensive. Moreover, line straightness

is critical for precise and high-resolution printing. In the manual approach, the quality response, q , was evaluated according to a line quality rank, as reported in **Table 2**. This protocol was tested, fine-tuned, and verified by five operators. In the automated procedure, the images were processed using a MatLab tool that analytically determines the mean and the standard deviation (σw_l and σw_o) of the line (w_l) and the overspray (w_o) width (**Figure 2A**). Using these quantities, the line quality, q_a , can be defined as:

$$q_a = u_1 \times \frac{\bar{w}_l}{\bar{w}_l + \bar{w}_o} + u_2 \times \frac{\bar{w}_l}{\bar{w}_l + \sigma w_l} + u_3 \tag{1}$$

In particular, the optimal value of the variables (u_1, u_2, u_3) is found by solving a least square problem, given by:

$$\min_{u_1, u_2, u_3} \| q_a - q_2 \| \tag{2}$$

The image processing procedure is composed of three main steps. First, the image contrast is enhanced to evidence the overspray and the line borders (**Figure 2B and C**). Then the line length is divided into $k = 13$ pieces (**Figure 2D**); for each of them, the minimal of the grayscale levels, corresponding to

Table 2. Qualitative line quality ranking from 1 (worst) to 5 (best), evaluated by optical microscopy (Hirox KH – 8700)

Quality rank (1-6)						
1	2	3	4	5	Reference-ideal case	

Quality rank (q): 1, sputtered line; 2, porous line with remarkable presence of overspray; 3, low dense and no straight line, with overspray; 4, dense but waved line, with overspray; 5, dense line and almost null overspray; Reference-ideal case - dense line and null overspray (indicative edited image).

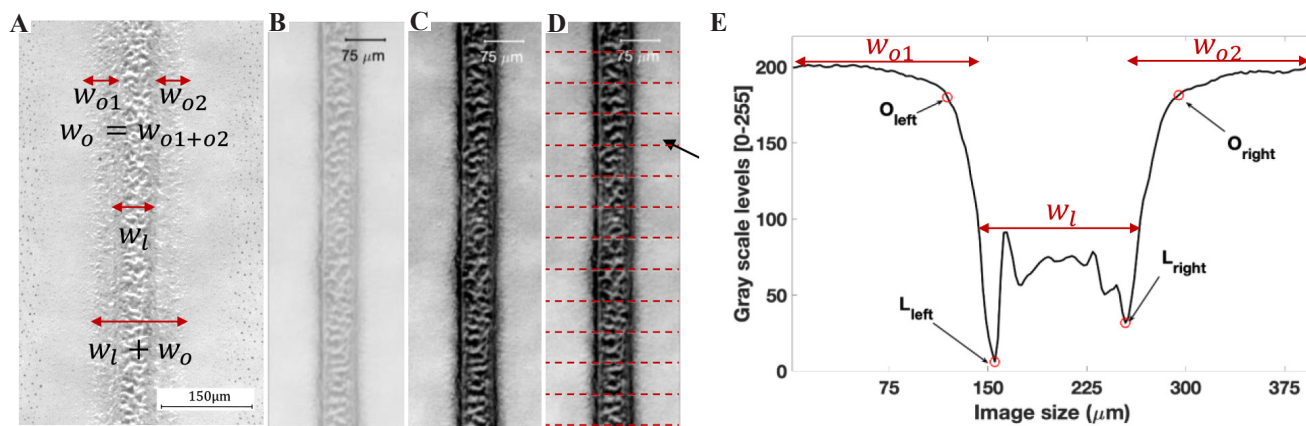


Figure 2. Quantitative image detection analysis. (A) Representative figure of a printed line, with emphasis on the terms w_l , w_o ($w_o = w_{o1} + w_{o2}$), and the total line with ($w_l + w_o$). (B) Original microscopic line image. (C) Line image with enhanced contrast. (D) Line length division (in red color) for analysis purposes. (E) Image size in μm plotted against the grayscale levels shows the printed line profile, w_l and w_o ($w_o = w_{o1} + w_{o2}$).

the two limits of the line (L_{left} and L_{right}), are retrieved. Furthermore, the overspray limits (O_{left} and O_{right}), defined as the ones for which the grayscale intensity reduces to 90% of the background, are computed (Figure 2E). The average line and the overspray width are then calculated as $\bar{w}_l = \sum_{i=1}^k w_l(i)$ and $\bar{w}_o = \sum_{i=1}^k w_o(i)$, where $w_l(i) = L_{right}(i) - L_{left}(i)$ and $w_o(i) = O_{right}(i) - O_{left}(i) - w_l(i)$.

2.3. Print technology transfer

In contrast to the typical empirical approaches applied to dedicated ink/substrate combinations, a methodology to allow direct transfer of printing strategies across different supports is proposed. It bases on the assumption Table 3. Contact angle (CA) images on glass slide and a NTE substrate, before and after plasma treatment, showing a comparable value of CA between glass slides and NTE substrates after plasma.

That, for a given ink, flat substrates (with low porosity) showing a similar surface energy would behave similarly during printing. Hence, the surface energies of the substrates were estimated via ink tests of known surface energy, γ_{TEST} (Series A, Tigres GmbH). As results, the glass slides showed a γ_G of 38 – 40 mN/m, while the Parylene-C-coated NTE substrates revealed a hydrophobic behavior and a γ_{NTE} of 32 – 34 mN/m. Hence, an oxygen plasma treatment (intensity 15 s/cm², offset ~ 8 mm, power 150 W, Plasma T-SPOT, Tigres GmbH) was applied on the substrates to match the surface energy of the glass slides. After treatment, the surface energy of the NTE support, $\gamma_{NTE-Plasma}$, was 40-42 mN/m. The ink-substrates wettability was also checked through CA. The CA tests were conducted by means of an OCA 15 plus system, equipped with a 25 gauge, 1 – 1/2" blunt needle (Nordson 7018339), and a 2 μ L sessile drop. Two CA repetitions on three samples of the substrates were recorded and fitted until the measurements were stable (~ 10 s). Table 3 reports the CA results on the glass slide and a NTE substrate. The data are comparable to each other. This should ensure transferability of the printing strategies. Note that possible temperature phenomena during printing due to the platen temperature were

Table 3. Contact angle measurement

Glass	NTE substrate <i>ante plasma</i>	NTE substrate <i>post plasma</i>
$\theta_1 = 44.05^\circ \pm 3.$	$\theta_2 = 52.79^\circ \pm 3.$	$\theta_3 = 46.24^\circ \pm 8.2$
		

neglected, considering that both glass and Parylene-C have low thermal conductivity.

2.4. Biocompatibility and cellular adhesion

The biocompatibility of the NTE substrate has been proven by Ferraro *et al.*^[27]. Additional immunofluorescence and cell viability assays were applied to test the biocompatibility and cellular adhesion on the Parylene-C coated NTE substrate and PEDOT: PSS samples. Specifically, immunofluorescence was executed to observe the cellular morphology and adhesion (nuclei and cytoskeleton) of human fibroblasts (HFs) and of human iPSCs derived neural stem cells (NSCs) on the Parylene-C-coated NTE substrate, along with tests of NSCs on Matrigel-coated PEDOT: PSS samples. Cell viability assays (direct and indirect) were instead executed to evaluate the cellular viability and proliferation of NSCs on the PEDOT: PSS samples only. Before cell seeding, all the samples were washed in phosphate-buffered saline solution (PBS) and further sterilized in an autoclave at 121°C for 20 min.

(1) Immunofluorescence of the Parylene-C-coated NTE substrates

Immunofluorescence with HFs

A preliminary immunofluorescence assay with HFs was performed on the NTE substrates covered with Parylene-C before and after oxygen plasma treatment (3 replicas) to test the performance of the treatment. A HF cell suspension (BJ cell line ATCC® CRL-2522™) at a concentration of 1×10^5 cells cm⁻² was poured onto the substrates with the addition of complete DMEM (DMEM supplemented with 10% fetal calf serum and 100 units/mL penicillin/streptomycin, Euroclone), and incubated for 30 min. After 4 days in culture, the cell culture was secured using the Fix&Perm Sample Kit® (SIC) to allow the fixation and the permeabilization of the cells (15 min each step) for a total time of 30 min. Subsequently, the specimens were incubated for 45 min with a blocking solution (iBind™ ×5 Buffer, Invitrogen), and further stained with Phalloidin (Sigma Aldrich), to detect the cellular cytoskeletal components. Later, cellular nuclei were counterstained for 5 min with the compound Hoechst 33342. Eventually, the specimens were positioned on glass coverslips on a drop of glycerol and studied by means of an inverted fluorescence microscope (Olympus IX70). Image analysis was performed via the Image-Pro Plus software v.7.0 (Media Cybernetics).

Immunofluorescence with NSCs

A second immunofluorescence assay was executed to test the adhesion and proliferation of NSCs on plasma-treated

Parylene-C-coated NTE substrates (3 replicas). Matrigel (Corning) was drop casted on the substrates and left for 1 h at 37°C. A line of human (hiPSCs) was reprogrammed, characterized, and differentiated in NSCs, by following the procedure presented by Ferraro *et al.*^[30]. A 100 µm strainer (Fisher Scientific) was used to filter the NSCs to achieve a single cell suspension. Subsequently, the cells were plated at a concentration of 1×10^5 cells cm⁻² on the specimens, including the control. After 30 min of incubation, a proper volume of Neural Expansion Medium (PSC Neural Induction Medium diluted 1:1 with Advanced DMEM/F-12 Thermo-Fisher Scientific) was added to each specimen. The well-plate was then incubated at 37°C in an atmosphere at 5% CO₂. After 24 h and 5 days of culture, cells were fixed and further analyzed following the same procedure adopted for HF_s, as previously described.

(2) Immunofluorescence of PEDOT: PSS samples

An additional immunofluorescence assay with hiPSC-derived NSCs was performed on two samples each of Matrigel-coated PEDOT: PSS ink and plastic, as control. The ink was printed in a square shape of 8 × 8 mm, with the combination of parameters: $\varnothing_{\text{nozzle}} = 300 \mu\text{m}$, $s = 25 \text{ mm/min}$, $A = 40 \text{ sccm}$, $S = 80 \text{ sccm}$, $T = 40^\circ\text{C}$, and for 20 layers. Post-printing curing was performed in a thermal oven (Heraeus) at $T = 150^\circ\text{C}$ for 8 min. Later, Matrigel (Thermo-Fisher Scientific) was drop casted on each sample for 1 h at 37°C. NSCs were filtered with a 100 µm strainer (Fisher Scientific) in order to collect a single cell suspension. Cells were then plated at a concentration of 5×10^4 cells cm⁻² and later deposited on the substrates. The samples were incubated for 30 min and eventually filled with an adequate volume of Neural Expansion Medium (Thermo-Fisher Scientific). The well-plate was finally incubated at 37°C in an atmosphere at 5% CO₂, over a period of 4 days. The same procedure for the NTE substrates was then applied to these specimens.

(3) Cell viability assay on NSCs

Cell viability was executed to evaluate the cellular viability and proliferation of NSCs on PEDOT: PSS printed samples. The presence of the DEG co-solvent might indeed affect the biocompatibility of the final printed pattern, despite the post-curing process that should allow its complete evaporation. In the literature, a couple of studies have demonstrated that DEG and its primary metabolite diglycolic acid are toxicants^[31]. Reed *et al.*^[32] stated DEG at high concentrations (100 mmol/L) induces the necrosis of SH-SY5Y neuroblastoma cells at 120 h already. However, to the best of the authors' knowledge, no research has ever been performed on PEDOT: PSS-based inks containing DEG in percentages of 12–20 wt%. The samples used were AJ[®] printed, cured, and coated with Matrigel, following the same procedure applied for the immunofluorescence assay on the PEDOT: PSS

ink. Biocompatibility was estimated by a direct rATP assay (CellTiter-Glo[®] 3D Cell Viability, Promega cat. no. G9681) and performed at 24, 48, and 96 h (three replicas each), including plastic as positive control. In details, this assay measures the quantity of viable cells by quantifying the adenosine triphosphate (ATP) values present in each well. ATP is recognized as a marker for metabolic cellular activity. A preliminary experiment was conducted to identify the suitable cell concentration to be cultured in order to reach a desirable amount of confluence (70–80%). From this analysis, a concentrated NSCs suspension of 6×10^4 cells cm⁻² was selected. Cells, previously kept at 37°C in an incubator, were detached, counted, seeded onto each sample, and further incubated for a period of 30 min. Later, each well was filled with a proper amount of neural expansion medium and incubated at 37°C and in a 5% CO₂ atmosphere. The ATP assay was performed according to supplier protocols after 24, 48, and 96 h of culture on triplicated samples. Briefly, a volume of CellTiter-Glo 3D Reagent equal to the volume of cell culture medium present in each well was added to induce cell lysis. After incubation at room temperature for 25 min to stabilize the luminescent signal, the total volume was transferred into a 96-well opaque-walled multiwell plate and the luminescence was recorded using Microplate Reader Infinite 200 (Tecan). Afterward, an ATP standard curve was plotted in the range of 10 µM to 10 nM, using the ribonucleoside triphosphate rATP (Promega cat. no. P1132) as positive control to compare the luminescence values acquired from the standard wells and the samples. Hence, the ATP concentration was calculated and plotted. To assess the material biocompatibility at multiple conditions of use, indirect rATP assays were also performed. In particular, PEDOT: PSS samples on Parylene-C-coated NTE substrates of 1 cm² were placed in a 24-well plate and let to release any potential cytotoxic components into 1 mL of Neural Expansion Medium for 5 days in a humidified incubator at 37°C and in 5% CO₂ atmosphere. As reference, the same volume of medium was poured in an empty dish and placed in the incubator at the same conditions. The day before the test, NSCs were seeded either in flat bottom 48-well plates Matrigel-coated (5×10^4 cell/well). Three replicates were set up for each condition. The day after, cell supernatant was removed and replaced by either ink sample conditioned medium or control medium. As experimental positive control NSCs were also seeded in fresh medium to verify that the neural medium, maintained at 37°C for 5 days, could not affect the cell healthy. Finally, the cells seeded in the 48-well plates were subjected to an ATP cell viability assay, as previously described for the direct rATP. Tests were conducted on both printed and spin coated PEDOT: PSS samples, and at different conditions of temperature and

annealing time to validate the findings regardless the amount of material deposited (dose-dependent behavior) and post-processing strategies.

2.5. Target application

Figure 3A schematically depicts the elements and functional principle of the intended device, which includes

two couples of in series capacitors for the generation of an alternated homogeneous spatial electric field across the microchannels patterned in the Si-based wafer. The final aim is to stimulate orientation and cells morphology along the channels by applying a combined uniaxial and bidirectional electrical-topographical cue. Figure 3B shows the entire fabrication procedure and Figure 3C

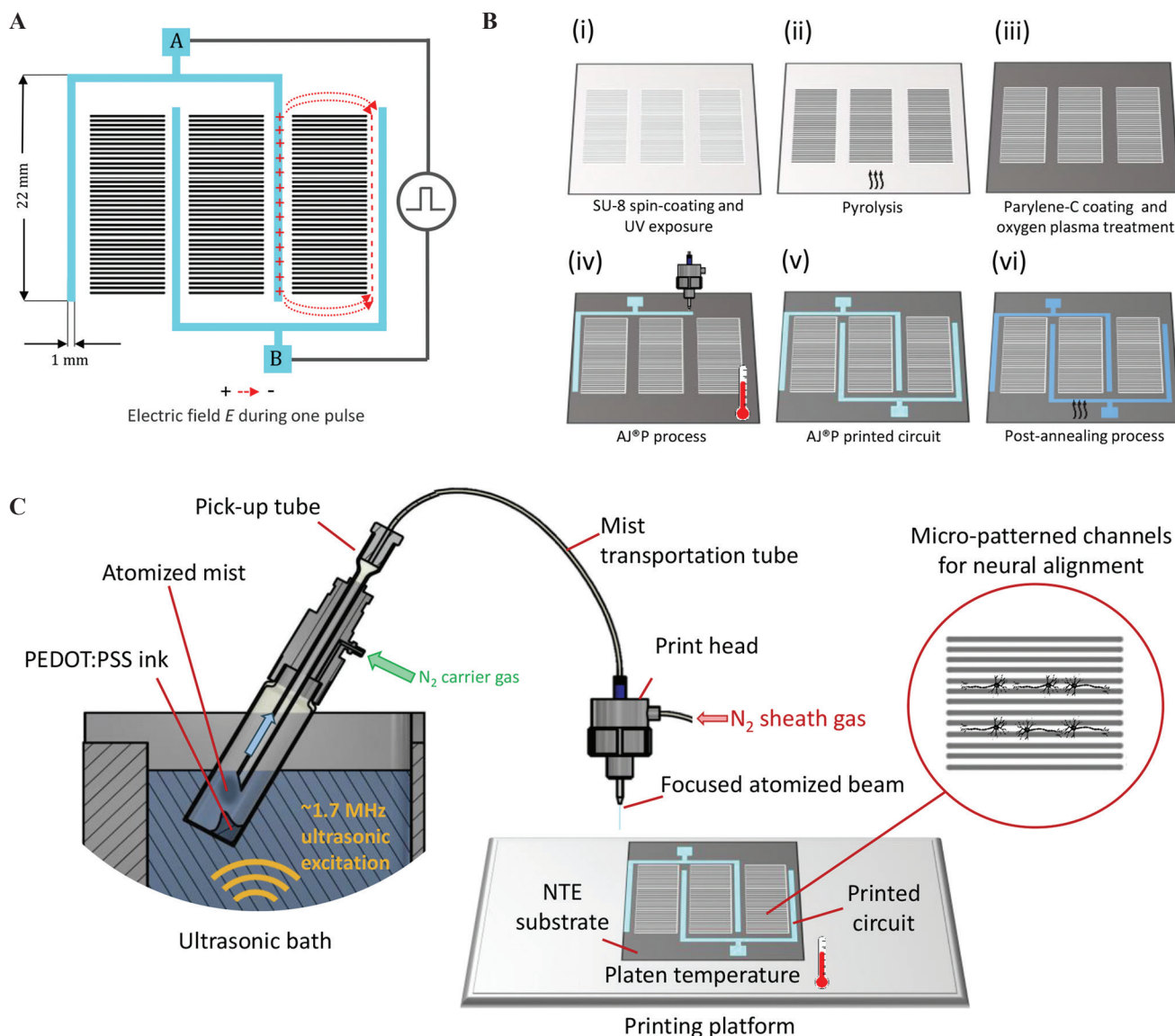


Figure 3. Aerosol Jet® Printing (AJ®P) process on the NTE substrate. (A) Schematic design of the bioelectrical integrated device for electrical and morphological stimulation, with the printed pattern (light blue color) around the micro-patterned channels (black color) on the NTE substrate. (B) Representation of the entire fabrication procedure of the device: (i) Fabrication of the microchannels via photolithography, including spin coating and ultraviolet exposure of the SU-8 photoresistor; (ii) pyrolysis treatment of the micropatterned substrate to obtain glassy carbon microchannels; (iii) Parylene-C coating and subsequent oxygen plasma treatment of the substrate; (iv) AJ®P of conductive patterns using a commercial inkjet PEDOT: PSS ink on the preheated substrate; (v) the AJ®P printed circuit before and (iv) after annealing in a thermal oven at 140°C for 1 h. (C) Schematic figure of the AJ®P on the Parylene-C-coated NTE substrate. Firstly, the PEDOT: PSS ink is atomized from liquid to mist in a glass vial positioned in the ultrasonic bath. Secondly, the mist is transported by a carrier gas into a transportation PTFE tube, and consequently focused by an annular sheath gas in the print head. The focused aerosolized beam is then printed according to the design pattern on the NTE substrate, located on the printing platform at a selected platen temperature. Figure adapted from Degryse et al., International Conference on Biofabrication, 2021^[33].

focuses on the AJ[®]P printing process of the circuit (light blue color) around the micro-patterned channels on the NTE substrate. Profilometer analyses of the printed electrical patterns (three repetitions) were performed by means of a DektakXT Stylus Profiler (Bruker, USA). The electrical impedance of the printed device was measured in PBS (Sigma Aldrich, BE) at a concentration of 10× and pH 7.4, using Potentiostat Gamry Reference 600 (Gamry Instruments, USA) (three repetitions). A 100 mV AC voltage was applied in the frequency range $1 - 5 \times 10^6$ Hz, with a delayed time of 10 s.

3. Results and discussion

3.1. Process investigation

Figure 4 shows the results of the line quality, q , on the glass substrate for T , A and S , where the tested focusing ratios, $R_f = A/S = (1, 1.5, 2)$, are highlighted with a circle. The experimental data are linearly interpolated and visualized in a contour plot. Regarding the analytical line quality q_a , it was detected that for quality ranks equal to $q_a \leq 2$ and $q_a = 5$ (i.e., the edges), the values obtained closely follow the visual quality ranks q . Instead, for quality ranks $3 \leq q_a \leq 4$, the results were ambiguous. At the current stage, the Matlab program developed in-house for automatic detection of the quality of printed lines is then able to reliably screen the best and worst results solely, according to the main purpose of high-quality printing. The issue related to quality ranks $3 \leq q_a \leq 4$ will be addressed in further studies. No single printed lines of ideal quality (reference-ideal case) could be obtained during the investigation, regardless the values of the process parameters. A certain amount of overspray is indeed intrinsic in AJ[®] printing. The aerosol beam is characterized by a non-uniform distribution of droplet size, and small, flying droplets, with high kinetic energy, will always diverge from the focused solid beam. For all three temperatures, no material deposition was detectable with the use of an $A = 10$ sccm. At $T = 25^\circ\text{C}$, lines of quality $q = 5$ were only achieved at the combination T25-A50-S100, while the rest was ranked as $q \leq 3$. Instead, when $T = 40^\circ\text{C}$, picks of quality $q = 5$ could be achieved at $A = 30$ and 40 sccm. Printed lines ranked with $q \geq 4$ were also attained when $A \geq 40$ sccm at 60°C . Moreover, the use of $R_f = 2$ generally gave thinner lines than the ones realized at $R_f = 1$. As an example, the line widths at T40-A40-S40 and T40-A40-S80 were $97 \mu\text{m}$ and $77 \mu\text{m}$, respectively.

A physical understanding of the process parameters and phenomena occurring during printing is here proposed to interpret the data. First of all, high R_f are most likely accompanied by a highly focused, thin solid beam which promotes the formation of well-designed

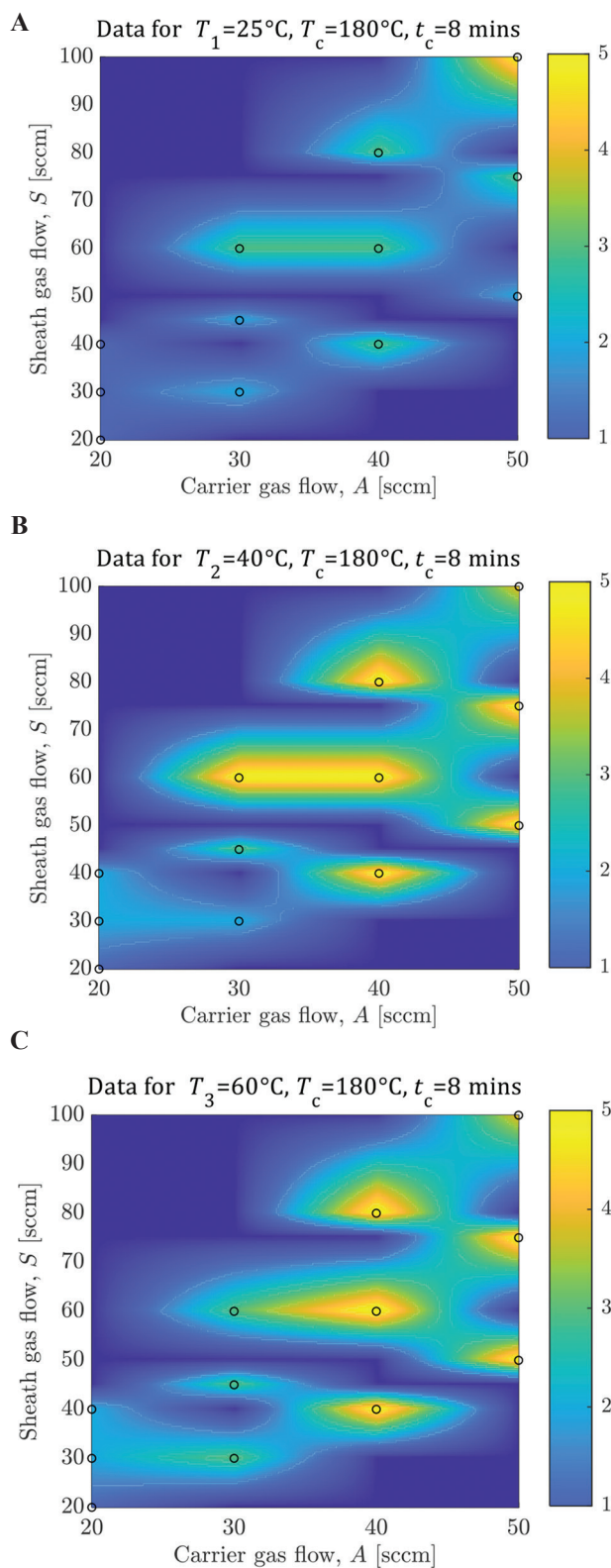


Figure 4. (A-C) Contour plot of line quality, q , from 1 (worst) to 5 (ideal) at $T = (25, 40, 60)^\circ\text{C}$ for $R_f = (1, 1.5, 2)$ with PEDOT: PSS ink and glass slides.

thin printed lines, while A has more likely effect on the kinetic energy and density of the aerosol beam. Hence, at low carrier gas flows, the aerosol will probably contain insufficient material to print dense features, while highly dense and energetic beams require large amount of sheet gas to be adequately focused. Secondly, a shrinkage of the PEDOT: PSS ink upon deposition was identified significant when $T = 60^\circ\text{C}$. This phenomenon is typically related to the ink composition. The ink used is indeed a mixed water-based solution with DEG as drying control agent (namely, co-solvent), at a low concentration of 12 – 20 wt%. In particular, DEG is known to possess a high boiling point and vapor pressure, and low surface tension. When the aerosolized ink impinges on the heated substrate at $T = 60^\circ\text{C}$, water evaporation is quickly enhanced, triggering a preliminary curing process, which starts from the surface of the deposited droplet of material. A convective flow toward the droplet center is then created (counter-clockwise Marangoni effect^[34]), typically resulting in the formation of a thin line, with curled/waved edges at low A ($q \leq 3$), and with cringed, dried-like surfaces at high A , despite straight edges ($q \geq 4$). Based on these observations, a flow rate of $A = 40$ sccm was chosen to speed the printing process, and a platen temperature, T , of 40°C was selected to allow for the coalescence of the printed wet layers. The combination of printed parameters $A40-S40$ and $A40-S80$ were finally designated and put forward for the next investigation.

The trend variations were then verified via additional tests conducted outside the initial process window and on the targeted substrate. **Figure 5** shows the results of R_{avg} and t_{avg} of printed interconnects and electrodes on glass slides and the Parylene-C-coated NTE substrates by varying n , when $T = 40^\circ\text{C}$. The thickness data were taken as average step height (ASH), considering the irregular profile of the printed features. The data were fitted by means of the following models: (i) $t_{avg} = c \cdot n$, being c a constant, and (ii) $R_{avg} = a/n$, being $a = \rho^*l/(wc)$, where ρ is the material resistivity, and l and w the length and width of the printed feature. The experimental data fit the physical models ($R^2 > 0.85$) well. Although being less accurate and stable, the average prediction of electrical resistance and electrode thickness on the Parylene-C-coated NTE substrates are also acceptable. This confirms that the print transfer methodology adopted is able to provide the first suitable print settings, hence reducing the time and material investment for process study and optimization. The electrode thickness values are comparable for both substrates; the effect of n is more remarkable when printing the electrodes; accordingly, the electrical resistances decay more rapidly, and suitable conductive features are attained already within ~ 15 layers, as in the usual practice of PE. The variation on the average thickness increases

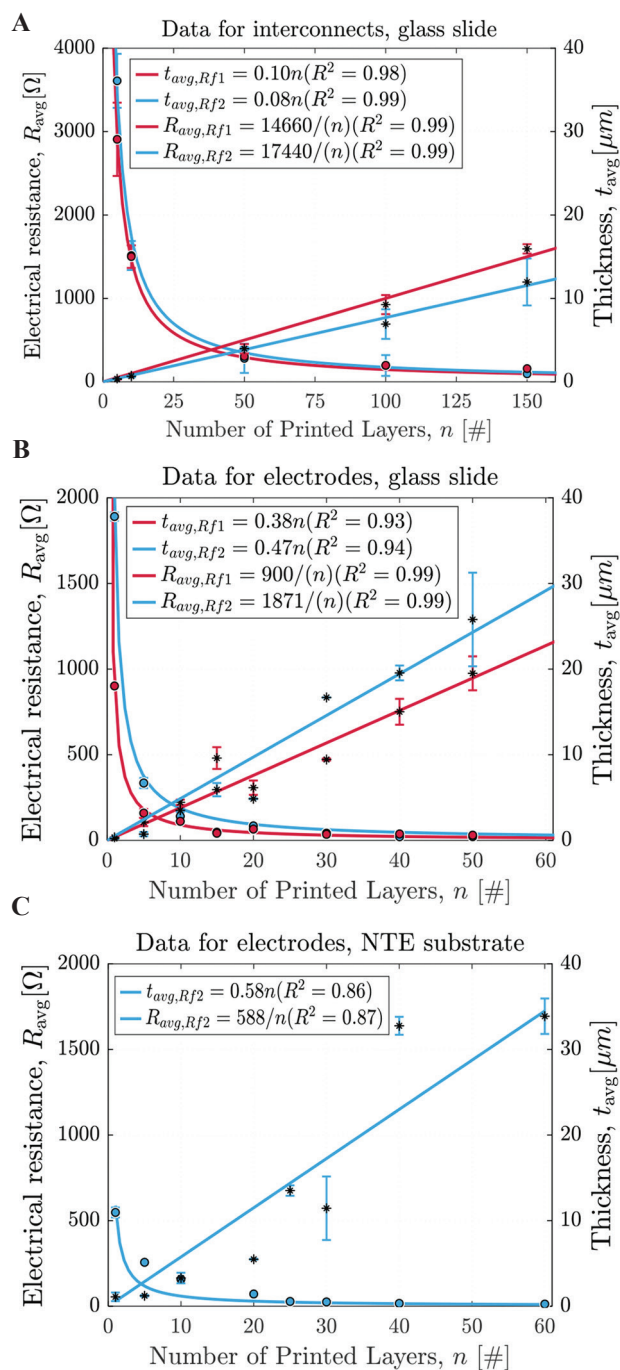


Figure 5. R_{avg} and t_{avg} of AJ[®]P PEDOT: PSS interconnects (single printed line) and electrodes on glass slides (A and B) and NTE substrates (C) at 40°C .

with n , and no evident effect of the R_f parameter could be noted on the thickness response. In this regard, it is to note that the ink used in this work is not recommended for high aspect ratio printing due to the low solid content and the type of co-solvent. This phenomenon is particularly evident when printing lines layer-by-layer. The irregular

profile of one deposition is reflected and cumulates with the successive one, leading to remarkable inaccuracy and inefficient build thickness.

Accordingly, a layer-by-layer print strategy of (thin) adjacent overlapped lines is typically recommended in PE to print well defined and solid lines. It is also to note that ink composition for 3D AJ[®]P micro-structuring is still under investigation within the research community but getting increasing interest. Eventually, the electrodes on the Parylene-C-coated NTE substrates have the lowest electrical resistance, given the highly insulating properties of the coating. This is beneficial for the reduction of the dispersion of the electrical signal.

3.2. Biocompatibility and cellular adhesion

(1) Immunofluorescence of the seeded Parylene-C-coated NTE substrates

Figure 6 shows the results of immunofluorescence performed on the Parylene-C-coated NTE substrates. In particular, the findings on HF^s seeded on untreated and oxygen plasma-treated substrates after 4 days of culturing are shown in **Figure 6A–D**, respectively.

The figures demonstrate a drastic change in the cellular adhesion between *ante* and *post* plasma treatment, which is in line with the literature. In particular, the NTE substrates *ante* plasma hindered the cellular adhesion and consequent proliferation and physiological metabolic activity. HF^s were indeed disposed in spherical agglomerates and associated to a possible suffering condition. On the contrary, the Parylene-C-coated NTE substrates *post* plasma showed successful HF^s adhesion, with consequent cellular spreading and colonization on the surface, enhancing their continuous and homogeneous alignment according to the desired geometry, that is, from a flat surface to microchannels. The Parylene-C-coated NTE substrates, *post* plasma and *post* Matrigel coating, also successfully sustained the adhesion and proliferation of NSC^s immediately after 24 h (**Figure 6E and F**). After 5 days of culturing, the cells were also able to proliferate and cover the entire surface homogeneously (**Figure 6G and H**). In particular, the NSC^s tended to align along the sidewalls of the conduits and connect across them. This result is comparable with other studies performed on different cell types, including neuronal cells^[35], and on shallow grooves^[36,37]. As reported by Trantidou *et al.*^[38], oxygen plasma causes intermolecular reactions for the formation of functionally charged groups, such as C=O, C-O, etc. In addition, Parylene-C treated with oxygen plasma (particularly with powers above 50W) maintains hydrophilicity saturation of ca. 40–50% from its initial state after 7 days^[38]. This is sufficient to allow for an initial cellular attachment and proliferation

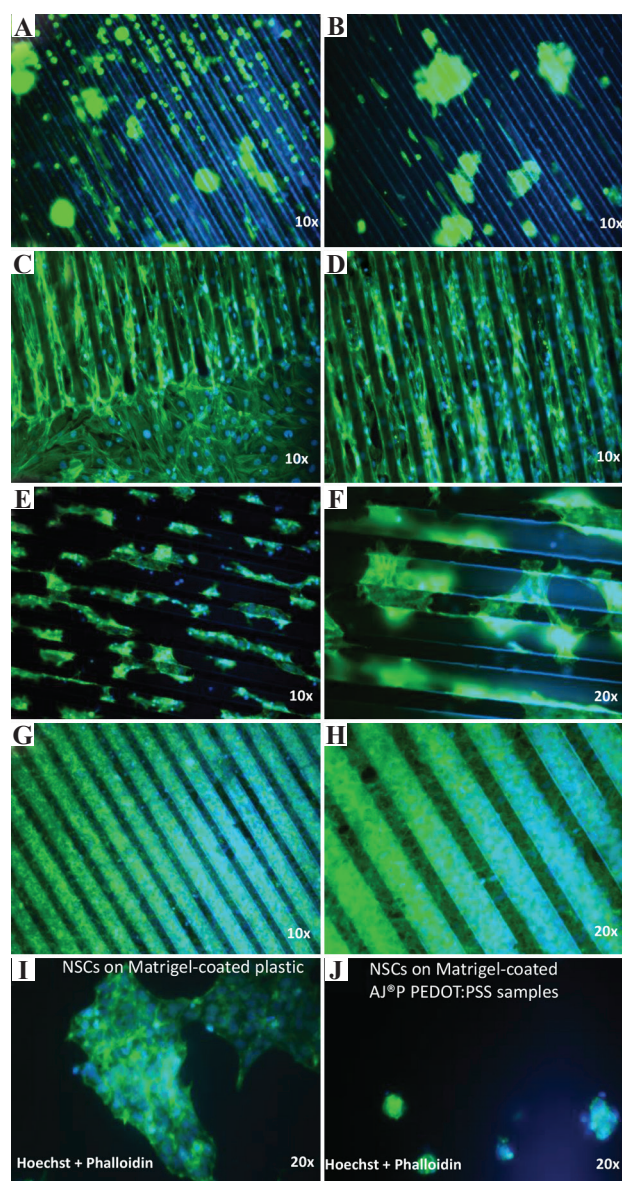


Figure 6. Immunofluorescence assays of HF^s on (A) NTE substrates *ante* plasma, showing a non-adhesion of HF^s, with (B) the presence of agglomerates in round-like shapes, detectable as an unhealthy cellular condition, and on (C) NTE substrates *post* plasma, representing good cellular adhesion of HF^s, with (D) HF^s aligned in the micro-channels, demonstrating the validity of the plasma treatment and the applied topographical cue. Immunofluorescence assays of NSC^s on Parylene-C-coated NTE substrates *post* plasma at 24 h, magnification $\times 10$ (E) and $\times 20$ (F), and at 120 h, magnification $\times 10$ (G) and $\times 20$ (H), showing good cellular adhesion and morphological alignment, with cellular network formation across the channels. Immunofluorescence assays of NSC^s on plastic control and PEDOT:PSS ink: (E) NSC^s cultured on Matrigel-coated plastic, showing good adhesion, (F) NSC^s cultured on Matrigel-coated AJ[®]P PEDOT:PSS samples, showing an unhealthy cellular state.

during the cell culturing period. The substrates can be therefore used for cellular topographical guidance.

(2) Cell adhesion and viability on PEDOT: PSS samples

As shown in **Figure 6I and J**, the immunofluorescence assays of NSCs cultured on Matrigel-coated AJ[®]P PEDOT: PSS printed samples show limited cellular adhesion and no detectable proliferation subsequently. This is in contrast with the data on NSCs seeded on Matrigel-coated plastic control samples, which exhibit a healthy state condition of cellular adhesion and proliferation along with neural networks formation. This can be caused by a detected hydrophobic behavior of the samples when in contact with the NSCs/medium culture dispersion. When poured on the samples, the NSC dispersion remained confined into a drop-like shape, limiting cell spreading on the surface (**Figure 7A**). A potential cytotoxicity of the used PEDOT: PSS ink can

be also a major (co-)cause of these results. At 48 h, a detectable presence of cellular agglomerates was visible near the well edges (**Figure 7B**). **Figure 7C** shows the findings of the cell viability rATP assay (time points 24 h, 48 h, and 96 h) of NSCs cultured on Matrigel-coated AJ[®]P printed PEDOT: PSS samples. At time point 24 h, NSCs showed a healthier state on the plastic control than on the sample. At 48 h, the metabolic activity of the NSCs on the substrates further reduced. Eventually, at 96 h, the cytotoxicity of the PEDOT: PSS samples was $\times 10$ higher than the plastic controls. This could be related to the residual presence of the co-solvent DEG in the printed pattern, which does not fully evaporate after sintering. To validate this hypothesis, an indirect cell viability assay was performed on printed PEDOT: PSS samples sintered

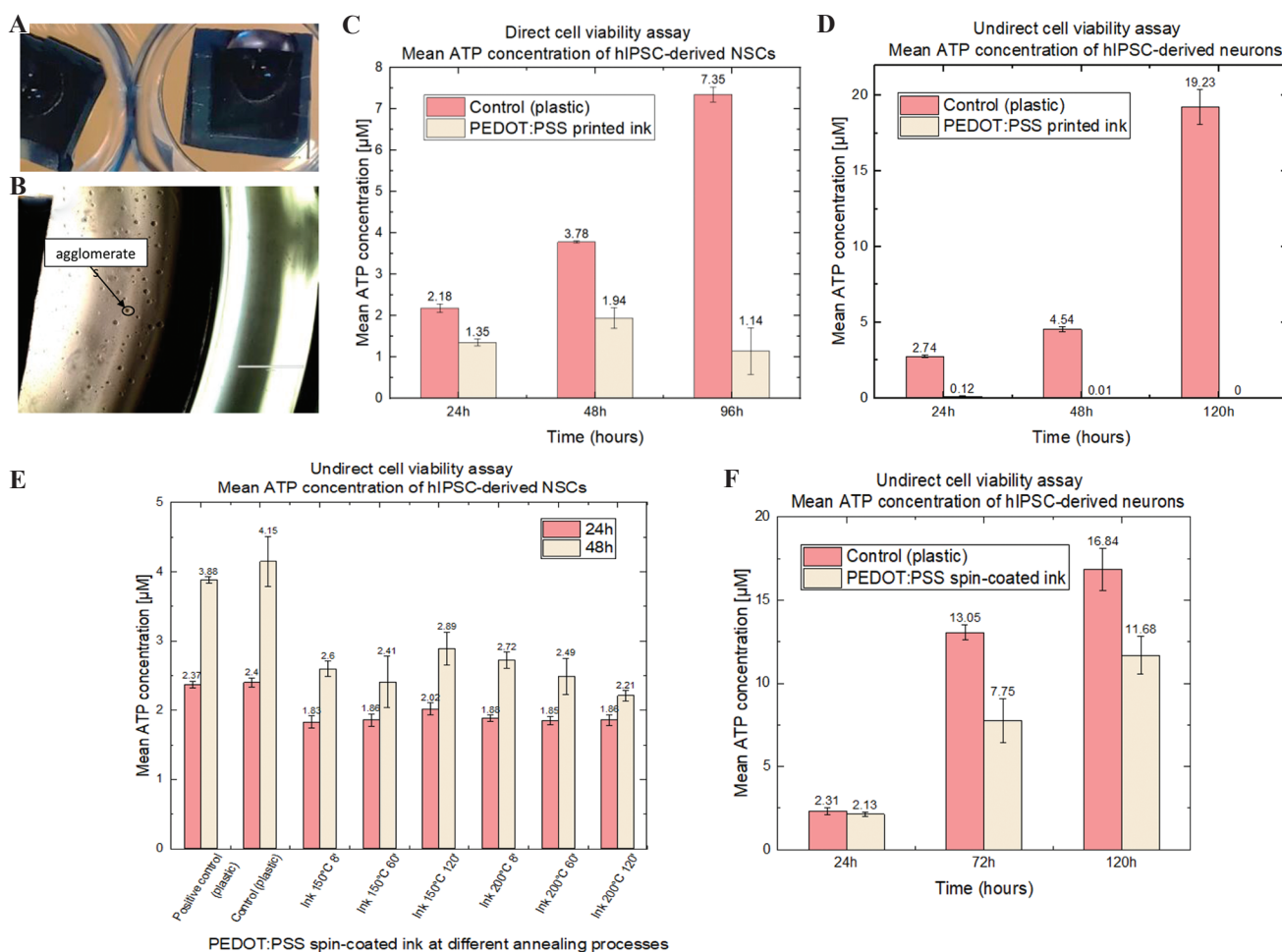


Figure 7. Cell viability assay of NSCs on plastic control and PEDOT: PSS samples. (A) Representative image of the ink’s hydrophobicity. (B) Optical image with focus on the presence of NSCs agglomerates near the well edges detected after 48 h. (C) NSCs rATP direct viability assay at 3 time points (24 h, 48 h and 96 h) on printed PEDOT: PSS samples, revealing an increasing cytotoxic behavior of the PEDOT: PSS ink. (D) NSCs rATP indirect viability assay at 3 time points (24 h, 48 h and 120 h) on printed PEDOT: PSS samples, confirming a high cytotoxic behavior of the PEDOT: PSS ink already after 24 h. (E) NSCs rATP indirect viability assay at 2 time points (24 h and 48 h) on spin-coated PEDOT: PSS samples, cured at six different conditions (150°C for 8, 60, and 120 min, and 200°C for 8, 60, and 120 min), showing good biocompatibility. (F) NSCs rATP indirect viability assay at 3 time points (24 h, 72 h, and 120 h) on spin-coated PEDOT: PSS samples, cured at 150°C for 120 min, confirming a dose-dependent behavior of the PEDOT: PSS ink.

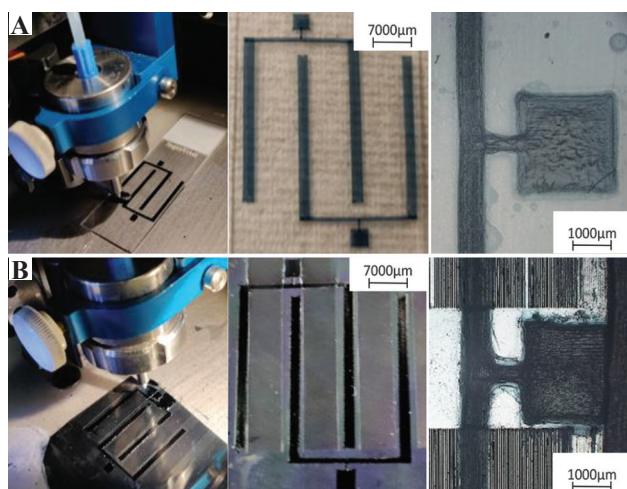


Figure 8. Printing of the device: on (A) glass substrate and (B) NTE substrate.

for a longer period of time (2 h against 8 min) at 150°C. The results confirmed the previous observations, showing a drastic cytotoxic ink behavior already after 24 h, with no value detected at the following points of 48 h and 120 h (**Figure 7D**). As such, the printed PEDOT: PSS ink is considered cytotoxic for NSCs.

To verify whether this ink behavior is related to a dose-dependent and/or sintering condition, additional indirect cell viability assays were carried out on nanometric spin-coated PEDOT: PSS samples, and at six different curing conditions (150°C for 8, 60, and 120 min, and 200°C for 8, 60, and 120 min). **Figure 7E** indicates that non-significant variations were detected among the different annealing conditions after 48 h. The conditions at 150°C and 120 min were then taken as reference settings for the preparation of the next spin-coated samples, and the ATP was tested up to 120 h. The results, shown in **Figure 7F**, confirm the hypothesis of a dose-dependent behaviour of the ink. Despite a significant reduction of the cellular viability at 48 h with respect to the plastic control (40.61% less), the biocompatibility of the nanometric spin-coated films was considered acceptable, resulting in 29.38% less biocompatibility than the plastic control at 120 h.

3.3. Target application

The printing strategy depicted in **Figure 5C** was ultimately applied to realize the target application. **Figure 8A and B** show images of the prototypes fabricated with AJ[®]P printed interconnects and electrodes on glass and Parylene-C-coated NTE substrates, respectively. Each electrode was ca. 33 µm thick and ca. 2 mm wide (including overspray), with an electrical resistance, $R = 16 \Omega$. **Figure 9** reports a characterization of the device printed on NTE substrates. In particular, **Figure 9A** displays the contour profile of AJ[®] printed

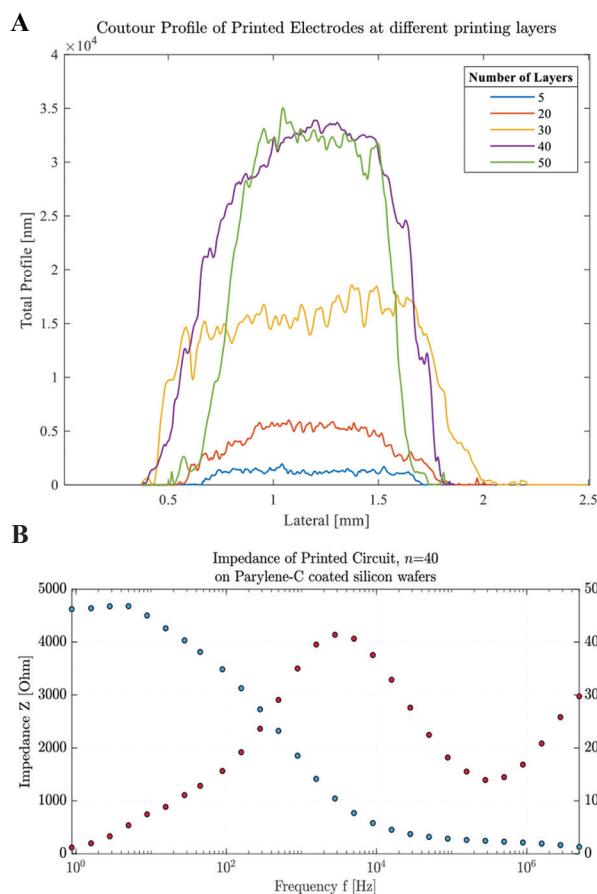


Figure 9. Characterization of the device: (A) Contour profile of printed electrodes at different printing layers $n=(5,20,30,40,50)$, showing the potentiality of reaching ca. 30 µm with $n=40$; (B) Electrical impedance of the printed circuit (40 layers) on Parylene-C NTE substrate. Impedance (Ω) and phase ($^\circ$) are plotted versus frequency (Hz).

electrodes at different printed layers, demonstrating the possibility to reach the same height of the micro-channels, ca. 30 µm, with the number of layers $n \geq 40$. Electrodes of the same height are indeed important for establishing a constant electrical field that is well aligned with the channel direction. In addition, **Figure 9B** depicts the electrical impedance of the printed device, showing that the behavior of the circuit correctly follows a theoretical RC circuit. In particular, the impedance was detected in the range of 1 – 2 k Ω at 1 kHz, in accordance with typical values of neural electrodes for detecting neural activity, demonstrating the validity of the device.

4. Conclusions

In NTE, multiple and complementary guidance cues, such as topographical, electrical, mechanical and/or biochemical ones, are typically applied on a neural scaffold to regulate neural cell activities for *in vitro* studies. This work concerns the potential of Aerosol

Jet® Printing as PEs technology for the development of a NTE integrated device for combined electrical and topographical axon guidance. Specifically, the study concerns the use of a commercial PEDOT: PSS ink for the production of up to 30 mm thick printed patterns on an innovative substrate, and the related characterization. In particular, the influence of critical process parameters, such as platen temperature and focusing ratio, on the quality of the printed features was firstly investigated for a combination of ink-substrate of reference. Hereafter, a best practice technique is established to allow direct transfer of the designated print strategy to the substrate of interest, hence reducing time and costs associated to process investigation and optimization. The methodology bases on the assumption that, for a given ink, substrates with comparable surface energy will behave similarly during printing. An automated procedure to detect the quality of printed lines is also proposed, as first step toward the development of optimized and controlled AJ®P strategies. Finally, the identified parameters for AJ® printing on the NTE substrates ($R_f = 2$, when $S = 80$ sccm, $A = 40$ sccm) are applied to the target application, and a first prototype of the device is manufactured and preliminarily characterized.

New insights concerning the biocompatibility of commercial PE inks are also learned. Despite the well-known biocompatibility of this material, NSCs viability assays on the selected commercial PEDOT: PSS ink shows cytotoxic values $\times 10$ more than plastic control. A dose-dependent release of toxic compounds, caused by the residual presence of the co-solvent DEG in the printed patterns after sintering is regarded here as the possible cause. Hence, a surface encapsulation of the printing patterns will be necessary to allow the applicability of the selected ink. Alternatively, own-developed biocompatible AJ®P PE PEDOT: PSS solutions should be pursued. Further tests (such as electrochemical assays) and use of the intended device will be the subject of future works.

To summarize, this study is the first step toward the manufacturing of bioelectrical devices via AJ®P technologies. This approach, when combined with engineered scaffold, can open completely new possibilities and frontiers in the field of bioelectrical devices for TE applications, and *in vitro* testing. In this context, it is also to note that AJ®P of collagen films has also been recently demonstrated; therefore, it is possible to realize bioelectrical applications in a single manufacturing operation^[13,14].

Acknowledgments

The authors gratefully acknowledge the Research Foundation Flanders (FWO) for the doctoral fellowship

granted to Miriam Seiti, 1SB1120N. The authors thank Frederik Ceysens (KU Leuven, ESAT) for Parylene-C coating and measurement of impedance, and UHasselt for the use of wettability and profilometer instruments. The authors also thank Jie Zhang, Akash Verma, and Mohit Sharma (KU Leuven) for the fruitful discussions.

Funding

FWO, doctoral fellowship n. 1SB1120N.

Conflict of interest

The authors declare no conflict of interest.

Author contributions

E.F., P.S.G., and E.C. guided and supervised the project. E.F., P.S.G., and M.S. designed and supervised the experiments. M.S., R.M.F., S.G., and M.R.V. conducted experiments and contributed intellectually to the scientific design of the project. M.S. and E.F. mainly wrote the manuscript. All authors contributed to the final manuscript and provided critical feedback.

References

1. Wang W, Lu Z, Li J, *et al.*, 2020, Engineering the Biological Performance of Hierarchical Nanostructured Poly (ϵ -Caprolactone) Scaffolds for Bone Tissue Engineering. *CIRP Ann*, 69:217–20.
2. Li GN, Hoffman-Kim D, 2008, Tissue-Engineered Platforms of Axon Guidance. *Tissue Eng B Rev*, 14:33–51. <https://doi.org/10.1089/teb.2007.0181>
3. Pires F, Ferreira Q, Rodrigues CAV, *et al.*, 2015, Neural Stem Cell Differentiation by Electrical Stimulation Using a Cross-Linked PEDOT Substrate: Expanding the use of Biocompatible Conjugated Conductive Polymers for Neural Tissue Engineering. *Biochim Biophys Acta*, 1850:1158–68.
4. Wilkinson NJ, Smith MAA, Kay RW, *et al.*, 2019, A Review of Aerosol Jet Printing-A Non-Traditional Hybrid Process for Micro-Manufacturing. *Int J Adv Manuf Technology*, 105:1–21.
5. Machiels J, Verma A, Appeltans R, *et al.*, 2021, Printed Electronics (PE) as an Enabling Technology To Realize Flexible Mass Customized Smart Applications, *Procedia CIRP*, 96:115–20.
6. Goh GL, Tay MF, Lee JM, *et al.*, 2021, Potential of Printed Electrodes for Electrochemical Impedance Spectroscopy (EIS): Toward Membrane Fouling Detection. *Adv Electron Mater*, 7:2100043. <https://doi.org/10.1002/aelm.202100043>

7. Cantù E, Tonello S, Abate G, *et al.*, 2018, Aerosol Jet Printed 3D Electrochemical Sensors for Protein Detection. *Sensors*, 18:3719.
<https://doi.org/10.3390/s18113719>
8. Agarwala S, Goh GL, Yeong WY, 2017, Optimizing Aerosol Jet Printing Process of Silver Ink for Printed Electronics. *IOP Conf Ser Mater Sci Eng*, 191:12027.
<https://doi.org/10.1088/1757-899X/191/1/012027>
9. Verheecke W, van Dyck M, Vogeler F, *et al.*, 2012, Optimizing Aerosol jet® Printing of Silver Interconnects on Polyimide Film for Embedded Electronics Applications. In: 8th International DAAAM Baltic Conference Industrial Engineering, p373–9.
10. Vogeler F, de Cuyper J, Ferraris E, 2015, Aerosol Jet Printed PEDOT: PSS Strain Gauges on FDM Printed Substrates. In: Proceedings of the 4M/ICOMM2015 Conference, p417–20.
11. Striani R, Stasi E, Giuri A, *et al.*, 2021, Development of an Innovative and Green Method to Obtain Nanoparticles in Aqueous Solution from Carbon-Based Waste Ashes. *Nanomaterials*, 11:1–15.
<https://doi.org/10.3390/nano11030577>
12. Parate K, Pola CC, Rangnekar SV, *et al.*, 2020, Aerosol-jet-Printed Graphene Electrochemical Histamine Sensors for Food Safety Monitoring. *2D Materials*, 7:034002.
13. Gibney R, Matthyssen S, Patterson J, *et al.*, 2017, The Human Cornea as a Model Tissue for Additive Biomanufacturing: A Review. *Procedia CIRP*, 65:56–63.
<https://doi.org/10.1016/j.procir.2017.04.040>
14. Gibney R, Patterson J, Ferraris E, 2021, High-Resolution Bioprinting of Recombinant Human Collagen Type III. *Polymers*, 13:2973.
15. Saleh MS, Hu C, Panat R, 2017, Three-Dimensional Microarchitected Materials and Devices Using Nanoparticle Assembly by Pointwise Spatial Printing. *Sci Adv*, 3:e1601986.
16. Zips S, Grob L, Rinklin P, *et al.*, 2019, Fully Printed μ -Needle Electrode Array from Conductive Polymer Ink for Bioelectronic Applications. *ACS Appl Mater Interfaces*, 11:32778–86.
17. Seiti M, Degryse O, Gibney R, *et al.*, 2021, Aerosol Jet® Printing of 3D Micropillars Using Multiple Materials, Solid Freeform Fabrication Symposium, 2-4 August, Virtual Event.
18. Kong YL, Gupta MK, Johnson BN, *et al.*, 2016, 3D Printed Bionic Nanodevices. *Nano Today*, 11:330–50.
19. Ferlauto L, D'Angelo AN, Vagni P, *et al.*, 2018, Development and Characterization of PEDOT: PSS/Alginate Soft Microelectrodes for Application in Neuroprosthetics. *Front Neurosci*, 12:648.
20. Heo DN, Lee SJ, Timsina R, *et al.*, 2019, Development of 3D Printable Conductive Hydrogel with Crystallized PEDOT: PSS for Neural Tissue Engineering. *Mater Sci Eng C*, 99:582–90.
21. Schander A, Tesmann T, Stokov S, *et al.*, 2016, *In-Vitro* Evaluation of the Long-Term Stability of PEDOT: PSS Coated Microelectrodes for Chronic Recording and Electrical Stimulation of Neurons. In: Annual International Conference of the IEEE Engineering in Medicine and Biology Society (EMBS), p6174–7.
22. Tarabella G, Vurro D, Lai S, *et al.*, 2019, Aerosol Jet Printing of PEDOT: PSS for Large Area Flexible Electronics. *Flex Printed Electron*, 5:014005.
23. Sun H, Wang K, Li Y, *et al.*, 2017, Quality Modeling of Printed Electronics in Aerosol Jet Printing Based on Microscopic Images. *J Manuf Sci Eng*, 139:071012.
<https://doi.org/10.1115/1.4035586>
24. Zhang H, Choi JP, Moon SK, *et al.*, 2020, A Hybrid Multi-Objective Optimization of Aerosol Jet Printing Process Via Response Surface Methodology. *Addit Manuf*, 33:101096.
<https://doi.org/10.1016/j.addma.2020.101096>
25. McShan D, Ray PC, Yu H, 2014, Molecular Toxicity Mechanism of Nanosilver. *J Food Drug Anal*, 22:116–27.
<https://doi.org/10.1016/j.jfda.2014.01.010>
26. Seiti M, Ginestra P, Ferraro RM, *et al.*, 2020, Nebulized Jet-Based Printing of Bio-Electrical Scaffolds for Neural Tissue Engineering: A Feasibility Study. *Biofabrication*, 12:025024.
<https://doi.org/10.1088/1758-5090/ab71e0>
27. Ferraro RM, Ginestra PS, Lanzi G, *et al.*, 2017, Production of Micro-patterned Substrates to Direct Human iPSCs-Derived Neural Stem Cells Orientation and Interaction. *Procedia CIRP*, 65:225–30.
<https://doi.org/10.1016/j.procir.2017.04.044>
28. Tan CP, Craighead HG, 2010, Surface Engineering and Patterning Using Parylene for Biological Applications. *Materials (Basel)*, 3:1803–32.
<https://doi.org/10.3390/ma3031803>
29. Hsu JM, Rieth L, Normann RA, *et al.*, 2009, Encapsulation of an Integrated Neural Interface Device with Parylene C. *IEEE Trans Biomed Eng*, 56:23–9.
<https://doi.org/10.1109/TBME.2008.2002155>
30. Ferraro RM, Lanzi G, Masneri S, *et al.*, 2019, Generation of Three iPSC Lines from Fibroblasts of a Patient with Aicardi Goutières Syndrome Mutated in TREX1. *Stem Cell Res*, 41:101580.
<https://doi.org/10.1016/j.scr.2019.101580>
31. Landry GM, Martin S, McMartin KE, 2011, Diglycolic acid is the Nephrotoxic Metabolite in Diethylene Glycol Poisoning Inducing Necrosis in Human Proximal Tubule Cells *In Vitro*.

- Toxicol Sci*, 124:35–44.
<https://doi.org/10.1093/toxsci/kfr204>
32. Reed KJ, Freeman DT, Landry GM, 2021, Diethylene Glycol and its Metabolites Induce Cell Death in SH-SY5Y Neuronal Cells *In Vitro*. *Toxicol In Vitro*, 75:105196.
<https://doi.org/10.1016/j.tiv.2021.105196>
33. Degryse O, Gibney R, Bloemen V, *et al.*, 2021, Collagen Composite Inks for Aerosol Jet® Printing in Bone Tissue Engineering Applications. Wollongong, Australia: Biofabrication Conference.
34. Park J, Moon J, 2006, Control of Colloidal Particle Deposit Patterns within Picoliter Droplets Ejected by Ink-Jet Printing. *Langmuir*, 22:3506–13.
<https://doi.org/10.1021/la053450j>
35. Delivopoulos E, Murray AF, 2011, Controlled Adhesion and Growth of Long Term Glial and Neuronal Cultures on Parylene-C. *PLoS One*, 6:25411.
<https://doi.org/10.1371/journal.pone.0025411>
36. Trantidou T, Rao C, Barrett H, *et al.*, 2014, Selective Hydrophilic Modification of Parylene C Films: A New Approach to Cell Micro-Patterning for Synthetic Biology Applications. *Biofabrication*, 6:025004.
<https://doi.org/10.1088/1758-5082/6/2/025004>
37. Wei L, Lakhtakia A, Roopnariane AP, *et al.*, 2010, Human Fibroblast Attachment on Fibrous Parylene-C Thin-Film Substrates. *Mater Sci Eng C*, 30:1252–9.
38. Trantidou T, Prodromakis T, Toumazou C, 2012, Oxygen Plasma Induced Hydrophilicity of Parylene-C Thin Films. *Appl Surf Sci*, 261:43–51.
<https://doi.org/10.1016/j.apsusc.2012.06.112>

Publisher's note

Whioce Publishing remains neutral with regard to jurisdictional claims in published maps and institutional affiliations